

# Technical Notes

TECHNICAL NOTES are short manuscripts describing new developments or important results of a preliminary nature. These Notes cannot exceed 6 manuscript pages and 3 figures; a page of text may be substituted for a figure and vice versa. After informal review by the editors, they may be published within a few months of the date of receipt. Style requirements are the same as for regular contributions (see inside back cover).

## Boundary-Layer Structure in Cylindrical Rocket Motors

J. Majdalani\*

Marquette University, Milwaukee, Wisconsin 53233

### Introduction

IN recent years the boundary-layer structure in solid rocket motors has received much attention in the rocket combustion stability community. This attention might be attributed to the role that it plays in connection with a number of combustion mechanisms that occur in the vicinity of the burning surface. On that account the focus of this Note will be to analyze the acoustic boundary-layer structure via two recent analytical models that have been shown to agree favorably with available numerical and experimental data in the forward half of a rocket chamber.<sup>1</sup> Historically, the first model was derived by Flandro<sup>2</sup> using the vorticity transport equation and regular perturbations. The second was derived by Majdalani and Van Moorhem<sup>1,3</sup> using the momentum equation and a composite-scale perturbation technique. Despite their dissimilar analytical expressions, both models have been shown to concur over a wide range of physical parameters.<sup>1</sup> The latter offers a compact expression for the velocity field where information about the boundary layer can be extracted explicitly. The current Note will exploit this feature to explain the influence of various flow variables and address several related issues, including the penetration depth of the rotational region, the peculiar Richardson overshoot,<sup>4</sup> and the phase difference between oscillatory pressure and velocity. The reader is cautioned that the present treatment will be applicable to laminar conditions only and may not apply to aft rocket motor sections where turbulence is more likely to exist. In fact, we expect our analytical formulations to overpredict the velocity's rotational wave amplitudes and depths obtained in turbulent regimes. For discussions concerned with turbulent behavior, the reader is referred to the Refs. 5–14 and the references therein.

### Analysis

#### Wave Characteristics

We begin by considering the time-dependent velocity derived in Ref. 1 [cf. Eq. (63)]. Using the same notation as in Ref. 1, we write

$$u^{(1)}(r, z, t) = \frac{\varepsilon_w}{\gamma} \left[ \underbrace{\sin(k_m z) \sin(k_m t)}_{\text{Irrotational part}} \underbrace{-\sin \theta \sin(k_m z \sin \theta) \exp \zeta \sin(k_m t + \Phi)}_{\substack{\text{Rotational part} \\ \text{Wave amplitude} \quad \text{Propagation}}} \right] + \mathcal{O}(M_b) \quad (1)$$

where

$$\begin{aligned} \zeta(r) &= \xi \eta(r) r^3 \csc^3 \theta, & \Phi(r) &= \pi^{-1} S r \ln \tan \frac{1}{2} \theta \\ \theta &= (\pi/2) r^2, & c &= \frac{3}{2} \\ \eta(r) &= -y[1 + cy^c (yr^{-1} - c \ln r)]^{-1} \end{aligned} \quad (2)$$

The time-dependent velocity consists of a linear juxtaposition of inviscid, irrotational and viscous, rotational fields. From Eq. (1) one can infer that the vortical wave amplitude is controlled by two terms: 1) an exponentially decaying term—made possible by retention of viscous effects—that diminishes with increasing distance from the wall and 2) a sinusoidal term—made possible by inclusion of downstream convection of unsteady vorticity by the mean flow—which, in addition to its monotonic decrease with  $r$ , varies harmonically with the streamwise coordinate. Because the exponentially decaying wave amplitude depends directly on  $\xi = \omega_0^2 \nu_0 R / V_b^3$ , increasing the viscosity causes the amplitude to decay more rapidly. The role of viscosity is hence to impede the inward penetration of vorticity. Equation (1) also indicates that the axial variation in the wave amplitude along the centerline is controlled exclusively by the acoustic field, whereas the radial variation is decreed by the rotational field. On a separate note, recalling that the phase of the rotational wave is uniform along lines where  $(k_m t + \Phi)$  is constant, Eq. (1) yields the radial speed of wave propagation. The latter can be readily determined to be equal to Culick's radial mean flow velocity.<sup>15</sup> The solution thus appears to exhibit the proper coupling between mean and time-dependent components.

#### Boundary-Layer Envelope

From Eq. (1), the rotational wave amplitude that controls the evolution of the acoustic boundary-layer envelope can be recognized to be

$$\|\bar{u}^{(1)}\| = (\varepsilon_w / \gamma) \sin \theta \sin(k_m z \sin \theta) \exp(\eta r^3 \csc^3 \theta / S_p) \quad (3)$$

where  $S_p = 1/\xi$  is the so-called penetration number.<sup>1</sup> The point directly above the wall where this amplitude reaches 1% of its irrotational counterpart defines the edge of the rotational boundary layer. In this case the point must be calculated by finding the root  $r_p$  of

$$\begin{aligned} &\sin[(\pi/2)r_p^2] \sin\{k_m z \sin[(\pi/2)r_p^2]\} \\ &\times \exp\{r_p^3 \csc^3[(\pi/2)r_p^2] \eta(r_p) / S_p\} - \alpha |\sin(k_m z)| = 0 \end{aligned} \quad (4)$$

where  $\alpha = 0.01$  defines the 99% based boundary-layer thickness. In general this penetration depth will depend on the penetration number, the mode number, and the axial location. The larger the

penetration number, the larger the penetration depth will be because of a smaller argument in the exponential term arising in Eq. (4). The upper limit on the boundary-layer thickness ( $y_{pm} = 1 - r_{pm}$ ) can be determined from the inviscid formulation of the penetration depth. Setting  $\nu_0 = 0$  in Eq. (4) precipitates

$$\sin[(\pi/2)r_{pm}^2] \sin\{k_m z \sin[(\pi/2)r_{pm}^2]\} - \alpha |\sin(k_m z)| = 0 \quad (5)$$

Equation (5) can be manipulated algebraically to provide a closed-form asymptotic expansion for the maximum penetration depth. Taking advantage of the fact that  $r_{pm} < 1$ , the 99% inviscid thickness

Received March 7, 1998; revision received Nov. 12, 1998; accepted for publication Jan. 6, 1999. Copyright © 1999 by J. Majdalani. Published by the American Institute of Aeronautics and Astronautics, Inc., with permission.

\*Assistant Professor, Department of Mechanical and Industrial Engineering. Member AIAA.

can be evaluated from a one-term perturbation expansion extruded from Eq. (5):

$$y_{pm} = 1 - \left[ \frac{4\alpha |\sin(k_m z)|}{\pi^2 k_m z} \right]^{\frac{1}{4}} + \mathcal{O}(r_{pm}^6) \quad (6)$$

Because the minimum possible  $y_{pm}$  is 74.8% at  $z = 0$ ,  $r_{pm}$  cannot exceed a value of 0.252. Subsequently, the maximum error associated with Eq. (6) can be calculated to be  $0.000259 \ll M_b$ . This error can affect the depth of penetration only in the third or fourth decimal places, a practically negligible contribution.

### Comparisons

In Ref. 1 a comparative study of time-dependent velocity profiles has indicated that both regular perturbation<sup>2</sup> and composite-scale models<sup>1</sup> exhibited similar velocity profiles. Naturally, one would expect their penetration depths to be in agreement as well. In fact, the penetration depths can be evaluated analytically and are compared in Fig. 1 to the numerical solution described in Ref. 1 for  $z^*/L = \frac{1}{2}$  and a wide range of  $Sr$  and  $Re_k$ . When plotted against  $S_p$ , entire families of curves, such as those shown in Fig. 1, collapse into single curves per axial location. This event allows us to condense all information about the penetration depth on one graph per oscillation mode. As borne out in Fig. 2, characteristic curves of penetration depths at several axial locations spanning the length of the chamber can be conveniently depicted for the fundamental oscillation mode. Collapsing the results onto a single graph provides unambiguous means to interpret the boundary-layer structure.

As can be inferred from Fig. 2, the dependence of the penetration depth on the axial location  $z$  is minute in the forward half of the chamber and becomes more pronounced in the aft half. The

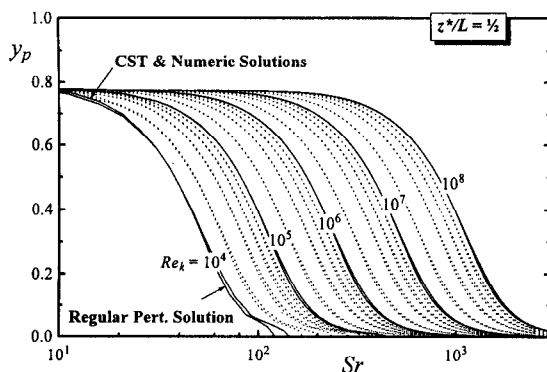


Fig. 1 Trace of the penetration depth obtained numerically and from two analytical models<sup>1,2</sup> for a wide range of control parameters and one axial station. CST, composite-scale technique.

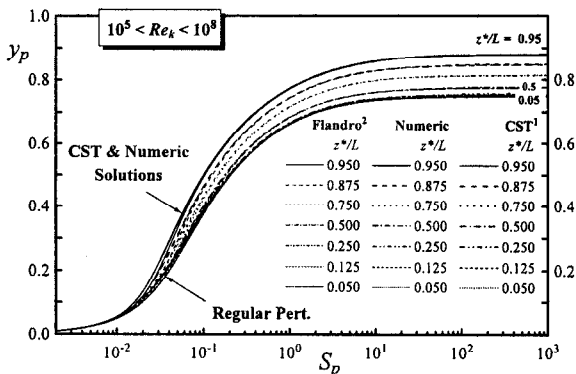


Fig. 2 Locus of the laminar penetration depth obtained numerically and from two analytical models<sup>1,2</sup> for a wide range of control parameters spanning the chamber length. The penetration of vorticity is expected to be less pronounced under turbulent conditions. CST, composite-scale technique.

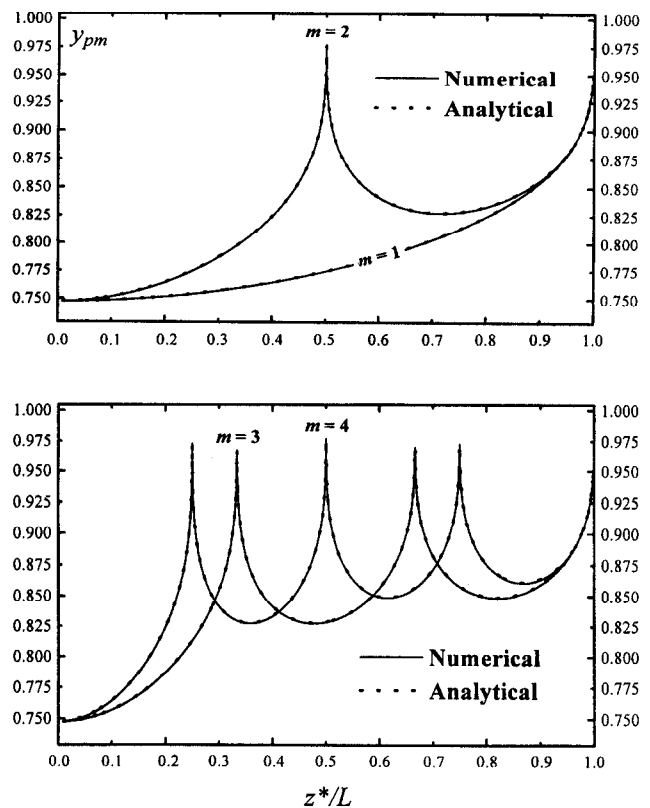


Fig. 3 Trace of the maximum penetration depth for the first four acoustic modes. Results correspond to laminar conditions that tend to overpredict the penetration depth in the chamber's aft half when turbulence is present.

increased sensitivity of the boundary-layer thickness to  $z$  with increasing axial distance from the head end is attributed to vortical intensification in the streamwise direction. For fundamental oscillation modes the axial dependence is found to be important only in the aft half of the chamber when  $z$  becomes relatively large. For small penetration numbers the penetration depth is found to be directly proportional to the penetration number, independently of the axial location. In practice this could take place when the mean flow injection speed is very small, resulting in insignificant vortical intensification in the streamwise direction. Evidently, this range does not correspond to rocket motors characterized by sizeable penetration numbers and, therefore, substantial penetration depths.

The sensitivity of the penetration depth to variations in the penetration number decreases at higher values of the penetration number associated with frictionless flows. As the penetration number becomes large, such as when exceeding 100 in Fig. 2, the value of the penetration depth becomes independent of the penetration number and can be estimated from the inviscid formulation given by Eq. (6). This maximum possible penetration depth  $y_{pm}$  that can occur at any axial location is compared in Fig. 3 with the numerical solution of Eq. (5) for the first four oscillation modes. Clearly, the maximum penetration depth increases with the axial location and the mode number. The axial increase is not monotone because  $y_{pm}$  reaches a maximum at the acoustic velocity nodes where the boundary layer extends to the core. The reader is cautioned that, because our current estimates correspond to laminar conditions, they tend to overpredict the penetration depth when  $z^*/L > \frac{1}{2}$ . In fact, in aft-rocket portions, the onset of turbulence has been shown to impede the vortical wave propagation. The reader is referred, for example to Fig. 13 in Ref. 13, where laminar and turbulent acoustic boundary layers are compared.

### Unsteady Velocity Overshoot

The phase difference between vortical and acoustic solutions causes a periodic overshoot of the time-dependent velocity that can

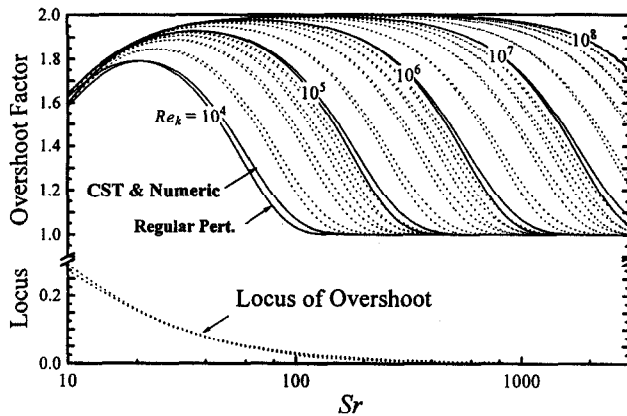


Fig. 4 Analytical<sup>1,2</sup> and numerical predictions of the locus and magnitude of Richardson's velocity overshoot at  $z^*/L = \frac{1}{2}$  and a wide range of control parameters. This overshoot is less intense under turbulent conditions. CST, composite-scale technique.

$$\beta_m(y=0) = \arctan \left[ \lim_{y \rightarrow 0} \frac{\xi \exp(-\xi y) \sin(-ySr) + Sr \exp(-\xi y) \cos(-ySr)}{\xi \exp(-\xi y) \cos(-ySr) - Sr \exp(-\xi y) \sin(-ySr)} \right] = \arctan(Sr S_p) \quad (10)$$

reach almost twice the acoustic wave amplitude. This overshoot is a well-known effect that is characteristic of oscillatory flows and was first discovered in experiments on sound waves in resonators by Richardson,<sup>4</sup> who first realized that maximum velocities occurred in the vicinity of the wall. Theoretical verifications of this peculiar phenomenon were carried out by Sexl,<sup>16</sup> and additional experiments were conducted by Richardson and Tyler<sup>17</sup> on reciprocating flows subjected to pure periodic motions.

In our problem the overshoot factor  $OF$  can be determined from Eq. (1) along with the distance  $y_{\max}$  extending from the wall to the point where maximum overshooting occurs. Figure 4 summarizes the observed trends that indicate that the overshoot increases with decreasing kinematic viscosity and frequency. The overshoot occurs in the vicinity of the wall, roughly, in the lower 25% of the solution domain. Indubitably, this corresponds to the most sensitive region near the burning surface. Because this overshoot is not captured by the one-dimensional model currently in use, the need to incorporate the two-dimensional field, presented here, becomes even more important, especially when proper coupling with the combustion process is desired near the propellant surface. When compared to the impermeable wall overshoot of about 113% (Ref. 18), the 200% magnification observed here is more significant. Plots of velocity overshoot and loci of these velocity extrema given in Fig. 4 are almost indistinguishable from corresponding numerical predictions. Note that the loci are independent of  $Re_k$  (i.e., viscosity) and depend only on  $Sr$ . For the regular perturbation model of  $\mathcal{O}(1/Sr)$ ,<sup>2</sup> slight deviations from numerical predictions can be discerned when  $OF < 1.75$  or  $Sr < 20$ .

#### Acoustic Pressure Phase Shift

In Eq. (1),  $\Phi(r)$  is the phase angle of the vortical velocity component with respect to the acoustic counterpart. This function is proportional to  $Sr$  and controls the propagation speed of the rotational wave. The angle  $\sigma_m$  by which the sinusoidal pressure wave leads the time-dependent velocity can be determined in the following fashion: First, the time-dependent pressure and velocities can be written as harmonic functions of time, viz.,  $p^{(1)} = \varepsilon_w \sin[k_m t + (\pi/2)] \cos(k_m z)$ , and

$$u^{(1)} = (\varepsilon_w / \gamma) \sqrt{(1 - A_m \cos \Phi)^2 + (A_m \sin \Phi)^2} \times \sin(k_m t + \beta_m) \sin(k_m z) \quad (7)$$

From Eq. (1),  $\beta_m = \arctan[-A_m \sin \Phi / (1 - A_m \cos \Phi)]$ , where

$$A_m = \sin[(\pi/2)r^2] [\sin(k_m z)]^{-1} \sin\{k_m z \sin[(\pi/2)r^2]\} \times \exp\{\xi \eta(r) r^3 \csc^3[(\pi/2)r^2]\} \quad (8)$$

Hence, for any axial location, the angle by which the pressure leads the velocity is simply  $\sigma_m = (\pi/2) - \beta_m$ . Near the wall the angle  $\Phi$  can be expressed in a Taylor-series form expanded about  $y = 0$ . The result is

$$\Phi(r) = \pi^{-1} Sr \ell_v \tan[(\pi/2)r^2] = Sr \left[-y + \frac{1}{2} y^2 + \mathcal{O}(y^3)\right] \simeq -ySr \quad (9)$$

The effective composite scale  $\eta$  that appears in Eq. (8) also exhibits an asymptotic form near the wall.<sup>1,3</sup> Indeed, because  $\eta(r) = -y$  at  $y = 0$ , the vortical velocity amplitude given by Eq. (8) simplifies to  $A_m = \exp[\xi \eta(r)] = \exp(-\xi y)$ . At the outset,  $\beta_m$  and  $\sigma_m$  become

$$\sigma_m(y=0) = \frac{\pi}{2} - \arctan(Sr S_p) = \frac{\pi}{2} - \arctan\left(\frac{V_b^2}{\omega_0 v_0}\right) = \frac{\pi}{2} - \arctan\left(\frac{V_b^2 L}{m \pi a_0 v_0}\right) \quad (11)$$

This exact analytical limit is common to all rotational models whether one dimensional<sup>3,19</sup> or two dimensional<sup>1,2,20</sup> and whether using purely analytical means,<sup>19</sup> regular perturbations,<sup>2,20</sup> or composite-scale techniques.<sup>1,3</sup> Furthermore, this limit can be verified by numerical computations. Near the centerline, where the acoustic velocity is the only nonzero component, the rotational velocity vanishes,  $\beta_m$  vanishes, and  $\sigma_m$  will be 90 deg. Thus, the acoustic pressure leads the velocity by an angle that varies from a small value at the wall to 90 deg at the centerline. Not unlike the velocity profile, there exists a phase overshoot that can reach 180 deg or twice the phase difference between acoustic pressure and velocity. By inspection of Eq. (11), the phase angle depends on the product of the Strouhal and penetration numbers. In dimensional form this product scales with the convection-to-diffusion-speed ratio of the rotational disturbances introduced at the wall. Lower injections, shorter chambers, higher oscillation modes, higher viscosities, or higher speeds of sound result in a larger pressure-to-velocity phase lead at the wall. The largest phase shift will occur, for instance, in a small solid rocket motor. Practically, this angle is a few degrees or less.

#### Relevance

The current analysis discloses the importance of the rotational flow component in altering the acoustic boundary-layer character. The actual structure of the boundary layer is quite different from the thin acoustic layer assumed in one-dimensional models. By analogy to Culick's steady flow solution,<sup>15</sup> the current solution could be incorporated into existing codes to improve prediction capabilities.

By analogy to the Stokes number that governs the thickness of the boundary layer in periodic flows with inert walls, the penetration number appears to play a similar role when the walls are made porous. In dimensional form this number  $S_p = V_b^3 \omega_0^{-2} v_0^{-1} R^{-1}$  indicates that the thickness of the acoustic boundary layer will depend chiefly on the injection velocity. The circular frequency is second in importance. Doubling the frequency decreases the penetration number by a factor of four, which, at sufficiently large frequencies, reduces the boundary-layer thickness by a factor of four also.

Because  $S_p$  is inversely proportional to  $\nu_0$ , viscosity plays the role of a wave-attenuation agent. Moreover, the chamber geometry appears to have an effect on the penetration number. In fact, decreasing the motor's effective radius causes the penetration depth to grow proportionately larger, which is to be expected because the effect of blowing becomes more appreciable when the cross-sectional area is reduced.

### Conclusions

The classical concepts of boundary-layer theory regarding inner, near-wall, and outer, external regions are almost reversed for unsteady flows over transpiring surfaces. Near the wall, instead of observing the traditionally thin viscous layer, a thick rotational layer is established near the solid boundary when sidewall injection is introduced, and this can be ascribed to the strong vortical transport in the radial direction. The acoustic boundary layer, in the context described here, is a region of highly concentrated vorticity. The corresponding penetration depth is, therefore, a measure of the vortical reach into the core. The thin layer where viscous friction is important is removed from the wall to the edge of the rotational region. The penetration depth appears to be a direct function of a similarity parameter that is 1) proportional to the cube of the injection speed, 2) inversely proportional to the square of the frequency, and 3) inversely proportional to the viscosity and chamber effective radius. This dependence is in agreement with empirical observations and numerical simulations. Finally, the pressure-to-velocity phase shift is found to vary from a few degrees or less at the wall to 90 deg along the core after undergoing a phase overshoot that is reminiscent of the Richardson effect. At the wall the phase shift is controlled by the quotient of the convection and diffusion speeds of the vortical waves.

### References

- <sup>1</sup>Majdalani, J., and Van Moorhem, W. K., "Improved Time-Dependent Flowfield Solution for Solid Rocket Motors," *AIAA Journal*, Vol. 36, No. 2, 1998, pp. 241–248.
- <sup>2</sup>Flandro, G. A., "On Flow Turning," AIAA Paper 95-2530, July 1995.
- <sup>3</sup>Majdalani, J., and Van Moorhem, W. K., "A Multiple-Scales Solution to the Acoustic Boundary Layer in Solid Rocket Motors," *Journal of Propulsion and Power*, Vol. 13, No. 2, 1997, pp. 186–193.
- <sup>4</sup>Richardson, E. G., "The Amplitude of Sound Waves in Resonators," *Proceedings of the Physical Society, London*, Vol. 40, No. 27, 1928, pp. 206–220.
- <sup>5</sup>Beddini, R. A., "Reacting Turbulent Boundary-Layer Approach to Solid Propellant Erosive Burning," *AIAA Journal*, Vol. 16, No. 9, 1978, pp. 898–905.
- <sup>6</sup>Beddini, R. A., "Injection-Induced Flows in Porous-Walled Ducts," *AIAA Journal*, Vol. 24, No. 11, 1986, pp. 1766–1773.
- <sup>7</sup>Beddini, R. A., and Roberts, T. A., "Tubularization of an Acoustic Boundary Layer on a Transpiring Surface," *AIAA Journal*, Vol. 26, No. 8, 1988, pp. 917–923.
- <sup>8</sup>Beddini, R. A., and Roberts, T. A., "Response of Propellant Combustion to a Turbulent Acoustic Boundary Layer," *Journal of Propulsion and Power*, Vol. 8, No. 2, 1992, pp. 290–296.
- <sup>9</sup>Cherng, D. L., Yang, V., and Kuo, K. K., "Numerical Study of Turbulent Reacting Flows in Solid-Propellant Ducted Rocket Combustors," *Journal of Propulsion and Power*, Vol. 5, No. 6, 1989, pp. 678–685.
- <sup>10</sup>Jarymowycz, T. A., Yang, V., and Kuo, K. K., "Numerical Study of Solid-Fuel Combustion Under Supersonic Crossflows," *Journal of Propulsion and Power*, Vol. 8, No. 2, 1992, pp. 346–353.
- <sup>11</sup>Tseng, I. S., and Yang, V., "Combustion of a Double-Base Homogeneous Propellant in a Rocket Motor," *Combustion and Flame*, Vol. 96, No. 4, 1994, pp. 325–342.
- <sup>12</sup>Roh, T. S., Tseng, I. S., and Yang, V., "Effects of Acoustic Oscillations on Flame Dynamics of Homogeneous Propellants in Rocket Motors," *Journal of Propulsion and Power*, Vol. 11, No. 4, 1995, pp. 640–650.
- <sup>13</sup>Apte, S., and Yang, V., "Effects of Acoustic Oscillations on Turbulent Flowfield in a Porous Chamber with Surface Transpiration," AIAA Paper 98-3219, July 1998.
- <sup>14</sup>Vuillot, F., and Avalon, G., "Acoustic Boundary Layer in Large Solid Propellant Rocket Motors Using Navier-Stokes Equations," *Journal of Propulsion and Power*, Vol. 7, No. 2, 1991, pp. 231–239.
- <sup>15</sup>Culick, F. E. C., "Rotational Axisymmetric Mean Flow and Damping of Acoustic Waves in a Solid Propellant Rocket," *AIAA Journal*, Vol. 4, No. 8, 1966, pp. 1462–1464.
- <sup>16</sup>Sexl, T., "Über den von E. G. Richardson Entdeckten 'Annulareffekt,'" *Zeitschrift für Physik*, Vol. 61, No. 6, 1930, pp. 349–362.
- <sup>17</sup>Richardson, E. G., and Tyler, E., "The Transverse Velocity Gradient near the Mouths of Pipes in Which an Alternating or Continuous Flow of Air is Established," *Proceedings of the Royal Society of London, Series A*, Vol. 42, No. 1, 1929, pp. 1–15.
- <sup>18</sup>Rott, N., *Theory of Time-Dependent Laminar Flows, High Speed Aerodynamics and Jet Propulsion—Theory of Laminar Flows*, Vol. 4, edited by F. K. Moore, Princeton Univ. Press, Princeton, NJ, 1964, pp. 395–438.
- <sup>19</sup>Flandro, G. A., "Effects of Vorticity Transport on Axial Acoustic Waves in a Solid Propellant Rocket Chamber," *Combustion Instabilities Driven by Thermo-Chemical Acoustic Sources*, edited by A. S. Hersh, I. Catton, and R. F. Keltie, Noise Control and Acoustics Vol. 4, American Society of Mechanical Engineers, New York, 1989, pp. 53–61.
- <sup>20</sup>Flandro, G. A., "Effects of Vorticity on Rocket Combustion Stability," *Journal of Propulsion and Power*, Vol. 11, No. 4, 1995, pp. 607–625.

S. K. Aggarwal  
Associate Editor